Solution Structure of an Analogue of Vasoactive Intestinal Peptide As Determined by Two-Dimensional NMR and Circular Dichroism Spectroscopies and Constrained Molecular Dynamics

David C. Fry,*,‡ Vincent S. Madison,‡ David R. Bolin,§ David N. Greeley,‡ Voldemar Toome,‡ and Bogda B. Wegrzynski‡

Departments of Physical Chemistry and Peptide Research, Hoffmann-La Roche Inc., Nutley, New Jersey 07110

Received August 3, 1988; Revised Manuscript Received October 27, 1988

ABSTRACT: Structures have been determined for a potent analogue of vasoactive intestinal peptide (VIP), Ac-[Lys^{12},Lys^{14},Nle^{17},Val^{26},Thr^{28}]VIP (VIP′), in methanol/water solutions. In CD studies, both VIP and VIP′ were helical in methanol/water, with the percentage of α-helix increasing with percentage methanol. The pH had little effect on the structure. Complete ^{1}H NMR assignments were made for VIP′ in 25% methanol at pH 4 and 6 and in 50% methanol at pH 6, using two-dimensional COSY, NOESY, and relay–COSY experiments. There were no widespread changes in chemical shifts between the samples at pH 4 and 6; however, widespread changes were observed between the samples in 25% and 50% methanol. Complete sets of NOEs were obtained for VIP′ in 25% methanol, pH 4, and in 50% methanol, pH 6. These NOEs were converted into distance constraints and applied in molecular dynamics and energy minimization calculations using the program CHARMM. A set of low-energy structures was obtained for VIP′ in each solvent system. In 25% methanol, VIP′ has two helical segments at residues 9–17 and 23–28. The remainder of the structure is not well determined. In 50% methanol, residues 8–26 form a regular, well-defined α-helix and residues 5–8 form a type III β-turn. The remaining residues are not ordered. These structural assessments agree with the CD data. In the lowest energy structure in 50% methanol, the side chains of Asp^3, Phe^6, Thr^7, and Tyr^{10} are clustered together—these residues are conserved throughout the family of peptide hormones homologous to VIP.

Vasoactive intestinal peptide (VIP)[1] is a 28-residue peptide amide that was first isolated and characterized from porcine duodenum (Said & Mutt, 1972; Mutt & Said, 1974) and has since been found in a wide variety of tissues, including those of the lung (Dey et al., 1981), the brain (Suzuki et al., 1985), the reproductive organs (Alm et al., 1977), the peripheral nervous system (Said, 1980), and the heart (Yoshida et al., 1974). VIP exhibits numerous pharmacological properties, of which the best characterized is its potent activity as a bronchodilator (Matsuzaki et al., 1980). It is considered to be the major relaxant agent in human lung (Said et al., 1974). Attempts are being made to develop analogues of VIP that maximize this activity for potential use as bronchodilators.

Design of VIP analogues could be greatly aided by knowledge of the three-dimensional structure of the peptide. Attempts at crystallization of the peptide have been unsuccessful. The structural information available previous to this study consisted of CD and one-dimensional NMR investigations of VIP fragments in D_2O and DMSO (Bodanszky et al., 1974; Robinson et al., 1982; Fournier et al., 1982, 1984). These studies suggested that VIP possessed considerable helical content in organic solvents and that a peptide fragment corresponding to residues 15–28 had the capacity to adopt a helical conformation.

In order to obtain a more detailed structure, we have used two-dimensional NMR to study a potent synthetic analogue of VIP in methanol/water solutions. NMR has been shown to be capable of yielding solution structures for peptides and small proteins of up to approximately 130 residues (Williamson et al., 1985; Weber et al., 1985a; Wüthrich, 1986; Holak & Prestegard, 1986; Klevit & Waygood, 1986; Redfield & Dobson, 1988). The basis of peptide structural determination by NMR is typically the observation of a set of nuclear Overhauser effects (NOEs), primarily among the backbone protons, which indicate interproton distances of <5 Å. These numerous local constraints are then considered collectively to suggest larger structural elements that can accommodate all of the data. We have used CD spectroscopy as a complementary technique, since it provides a direct assessment of large secondary structural elements but cannot give detailed localized information with respect to the primary structure.

These two approaches provided a well-defined three-dimensional structure for the VIP analogue. In order to obtain a more detailed refinement of the structure, and to explore the range of conformations compatible with the CD and NMR data, we performed molecular dynamics calculations starting with a fully extended structure and applying distance constraints obtained from the NMR experiments. The final structures from several such calculations were evaluated in

‡ Department of Physical Chemistry.
§ Department of Peptide Research.

[1] Abbreviations: VIP, vasoactive intestinal peptide: His-Ser-Asp-Ala-Val-Phe-Thr-Asp-Asn-Tyr-Thr-Arg-Leu-Arg-Lys-Gln-Met-Ala-Val-Lys-Lys-Tyr-Leu-Asn-Ser-Ile-Leu-Asn-NH_2; VIP′, the analogue Ac-[Lys^{12},Lys^{14},Nle^{17},Val^{26},Thr^{28}]VIP; Nle, norleucine [$CH_3(CH_2)_3CH(NH_2)CO_2H$]; NOE, nuclear Overhauser effect; NMR, nuclear magnetic resonance; CD, circular dichroism; COSY, two-dimensional *J*-correlated NMR spectroscopy; NOESY, two-dimensional NOE NMR spectroscopy; A/D, analog to digital; DSS, sodium 4,4-dimethyl-4-silapentanesulfonate; FID, free induction decay; relay–COSY, extended COSY with relayed transfer of coherent magnetization; RD, relaxation delay; $\Delta\delta$, change in chemical shift; DMSO, dimethyl sulfoxide; DCC, *N*,*N*′-dicyclohexylcarbodiimide; HOBT, 1-hydroxybenzotriazole; TFA, trifluoroacetic acid; DIPEA, *N*,*N*-diisopropylethylamine; EDT, 1,2-ethanedithiol; $\langle P_\alpha \rangle$, probability of forming α-helix from the Chou–Fasman algorithm; $\langle P_\beta \rangle$, probability of forming β-strand.

0006-2960/89/0428-2399$01.50/0

terms of overall energetic favorability and extent of agreement with the NMR and CD data. We report the most likely three-dimensional structures for the VIP analogue in our solvent systems.

Experimental Procedures

Peptide Synthesis. The analogue used in this study was Ac[Lys^{12},Lys^{14},Nle^{17},Val^{26},Thr^{28}]VIP. (For brevity, the analogue will be referred to as VIP′.) It was synthesized by solid-phase methodology (Merrifield, 1963) on benzhydrylamine resin (Vega Biochemicals; 200–400 mesh, 1% DVB, 0.38 mmol/g). The first amino acid, Boc-Thr(Bzl), was derivatized onto the resin as the preformed symmetrical anhydride (Hagenmaier & Frank, 1972) by using DCC in CH_2Cl_2. Final loading on the resin was 0.17 mmol/g. Solid-phase synthesis was carried out on a Vega Model 250 semiautomated synthesizer. All amino acids were incorporated with the α-amino functions protected with the Boc group. Side-chain functional groups were protected as follows: Ser and Thr as benzyl ethers; Tyr as a 2,6-dichlorobenzyl ether; Lys as the 2-chlorobenzyloxycarbonyl derivative; Asp as a cyclohexyl ester; and His as the tosyl derivative. All residues except Asn and Gln were incorporated as preformed symmetrical anhydrides in CH_2Cl_2. Asn and Gln were incorporated as the preformed HOBT esters in 50% DMF/CH_2Cl_2 (Mojsov et al., 1980). The extent of coupling was routinely monitored after each cycle by using the Kaiser ninhydrin test (Kaiser et al., 1970). Incomplete reactions were double coupled until completion.

The general procedure for each synthetic cycle, based on 10–15 mL/g of resin, was as follows: (1) 1% EDT/CH_2Cl_2 (1 × 30 s); (2) 50% TFA/CH_2Cl_2 with 1% EDT (1 × 60 s); (3) 1% EDT/CH_2Cl_2 (1 × 30 s); (4) 50% TFA/CH_2Cl_2 with 1% EDT (1 × 900 s); (5) CH_2Cl_2 (1 × 30 s); (6) 2-propanol (1 × 30 s); (7 and 8) repeat steps 5 and 6; (9) CH_2Cl_2 (1 × 30 s); (10) 6% DIPEA/CH_2Cl_2 (2 × 120 s); (11) CH_2Cl_2 (1 × 30 s); (12) 2-propanol (1 × 30 s); (13 and 14) repeat steps 11 and 12; (15) CH_2Cl_2 (2 × 30 s); (16) coupling 2 equiv of activated amino acid (10 min–2 h); (17) 2-propanol (1 × 30 s); (18) CH_2Cl_2 (1 × 30 s); (19) repeat steps 17 and 18; (20) DMF (2 × 30 s); (21) CH_2Cl_2 (3 × 30 s).

After completion of the coupling of Boc-His(Tos), the peptide–resin was deblocked at the α-amino group by performing steps 1–15. The peptide was then acetylated by treatment with 3 mL of acetic anhydride in 6% DIPEA/CH_2Cl_2 for 30 min, washed, and dried under vacuum.

The peptide was deblocked and cleaved from the resin according to a modification of the two-step HF protocol of Tam et al. (1983). An aliquot of peptide–resin was treated with dimethyl sulfide/HF (3/1) for 2 h at 0 °C, evaporated to dryness, and treated with HF/anisole (9/1) for 50 min at 0 °C. The reaction mixture was evaporated under vacuum, washed with ether (2 × 30 mL) and EtOAc (2 × 30 mL), and then extracted with 10% AcOH (3 × 30 mL). The aqueous filtrate was lyophilized to a white powder.

The crude peptide was purified by preparative HPLC on an LDC system equipped with Constametric pumps, gradient master, and a Spectromonitor III UV detector. The peptide was applied to a Whatman Magnum-20 ODS-3 column (2 × 50 cm) and eluted with a linear gradient of 25–35% B (buffer A = 0.1% TFA/H_2O; buffer B = 0.1% TFA/CH_3CN) at 8.0 mL/min. The main peak was cut by analytical HPLC analysis of collected fractions, pooled, and lyophilized to a white powder.

Yield was 22%. FAB-MS: MW calculated, 3267.79; found, 3267.73. Amino acid analysis: Asp 4.10 (4), Thr 3.03 (3), Ser 1.97 (2), Glu 1.10 (1), Ala 2.06 (2), Val 2.62 (3), Leu 3.10 (3), norleucine 1.02 (1), Tyr 2.03 (2), Phe 0.92 (1), Lys 4.95 (5), His 1.06 (1).

CD Spectroscopy. CD spectra were measured on a Jasco J500A spectropolarimeter at ambient temperature. The instrument was calibrated by using *d*-10-camphorsulfonic acid in H_2O. Samples were run in 50 mM phosphate buffer at various pH values, and in various concentrations of methanol/water. The cell length was 0.01 dm, and the peptide concentration was 0.02 mM.

NMR Spectroscopy. The samples used for NMR consisted of 4 mM VIP′ in solvent systems with two different ratios of methanol/water: 50% CD_3OH/50% H_2O (or 50% CD_3OD/50% D_2O) and 25% CD_3OH/75% H_2O (or 25% CD_3OD/75% D_2O). The sample in 50% methanol was studied at pH 6.0, and the sample in 25% methanol at pH 4.0 and 6.0. Sample volumes were 0.7 mL. The pH was adjusted with dilute solutions of HCl (or DCl) and NaOH (or NaOD). CD_3OD (99.6%) and CD_3OH (99.2%) were purchased from MSD Isotopes; DCl (99%) and NaOD (99%) were from Aldrich; D_2O (99.96%) was from Wilmad. All pH values are uncorrected meter readings. Sample tubes (5 mm) were 535-PP from Wilmad; tight-fitting Teflon caps were used. Integrity of the peptide following long NMR runs was verified by HPLC.

NMR experiments were performed on a Varian XL-400 spectrometer operating at 399.806 MHz for observation of protons, using 15-bit A/D conversion and quadrature phase detection. Samples were maintained at 22.5 °C and were not spun. The 2-D experiments performed were COSY (Aue et al., 1976; Bax & Freeman, 1981; Wider et al., 1984), NOESY (Anil Kumar et al., 1980; Wider, et al., 1984;), and relay–COSY (Eich et al., 1982; Weber et al., 1985b), acquired in phase-sensitive mode (States et al., 1982). The 2-D experiments were collected as 256 t_1 experiments of 1024 points per FID, with spectral widths of 4000 Hz in each dimension and the carrier positioned at the water resonance (4.86 ppm), with an acquisition time of 0.128 s per transient. Relaxation delays of 1.0 s (COSY, NOESY) or 1.5 s (relay–COSY) preceded each transient, and the total number of transients was 64–96 (COSY, relay–COSY) or 240 (NOESY), with one or more initial dummy scans. In protonated solvents, suppression of the H_2O resonance was accomplished by preirradiation during the relaxation delay with the decoupler, which was set at 10 dB below 0.2 W. In order to observe samples in H_2O with the receiver gain set at optimal values, we inserted an attenuator (Kay 439A) between the probe and the receiver and typically applied 20–30 dB.

NOESY experiments were acquired with mixing times of 0.1, 0.15, 0.2, 0.3 and 0.4 s. Structural assessments utilized values from the 0.2-s experiment, since no secondary effects were observed at this mixing time. The two relay–COSY experiments (pulse sequence: $90°-t_1-90°-\tau_{relay}-180°-\tau_{relay}-90°-t_2$) that were found to be most useful employed τ_{relay} delays of 15 ms–15 ms and 30 ms–30 ms.

After acquisition, all data were transfered via Ethernet to a Vax 8800 computer, for processing with the program FTNMR (Hare Research, Inc.). Data from 2-D experiments were transformed by zero-filling to a final size of 1K × 1K real points and multiplying by a sine bell function extending to 350 points in the t_2 dimension, and a sine bell function extending to 256 points shifted by 0° (COSY, relay–COSY) or 50° (NOESY) in the t_1 dimension.

The exchange rates of NH protons in the samples were evaluated by using one-dimensional water saturation-transfer

experiments (Waelder & Redfield, 1977). These experiments utilized the pulse sequence (Rosevear, et al., 1985):

$$\{[\text{RD–preirradiation}(\omega_{H_2O})\text{–observation pulse}]_{16}\text{–}[\text{RD–preirradiation}(\omega_{control})\text{–observation pulse}]_{16}\}_4$$

where $\omega_{control}$ was 10.9 ppm, RD was 1.0 s, and preirradiation was performed for 2.5 s with the decoupler at 10 dB below 0.2 W. The spectral width was 7000 Hz, and the acquisition time was 1.5 s. A water-suppressing 45°–τ–45° observation pulse was utilized (Kime & Moore, 1983) with the carrier set near the downfield resonances at 7.1 ppm and $\tau = 5.55 \times 10^{-4}$ s.

Molecular Dynamics and Energy Minimization. Peptide structures were built and adjusted by using the Roche Interactive Molecular Graphics (RIMG) software package (Mueller et al., 1986). The CHARMM program system (version 19) (Brooks et al., 1983) was used for constrained energy minimization and molecular dynamics optimization of the structures in a manner similar to that which has been described (Brünger et al., 1987). The CHARMM version 18 parameters and energy functions were used except that the van der Waals radii of O and N atoms in neutral groups were increased by 0.1 Å and those in charged groups by 0.2 Å, and the explicit 10–12 hydrogen-bonding term was neglected. With these modifications satisifactory hydrogen-bonded geometries and energies were obtained for both neutral and charged groups. Constraints were used for interproton distances and to maintain planarity of peptide groups. For pairwise electrostatic energies, the dielectric constant was set to a value equal to the distance between the charges. Reduced formal charges of +0.25 were used for the nonneutral Asp and Lys side chains. Throughout, minimization was conducted by using 200 steepest descent steps followed by assumed-basis Newton–Raphson steps until the energy converged to 0.01 kcal/mol (up to 5000 steps).

All unambiguously assigned NOEs were measured and converted into distance constraints, by assuming that the distance between two protons (r) and the NOE between them ($\tilde{N}$) were related as $r \propto (1/\tilde{N})^{1/6}$. The correlation time and T_1 values were assumed to be uniform throughout the peptide. Classification of the NOE-derived distances was simplified as follows (with centering values in Å): LL (2.00); L (2.30); ML (2.55); M (2.80); SM (3.05); S (3.30); and SS (3.60). The distance ranges were standardized by assuming that contiguous NH_i–NH_{i+1} NOEs were generally near 2.8 Å, the value found in an α-helix. The allowed range about each centering value was ±0.50 Å, except for the SS constraint, for which the upper limit was +0.9 Å. The error values were chosen to accommodate the simplified two-spin model, the other assumptions previously described, and uncertainties in the NOE measurements, including the slight asymmetry that is unavoidable in any NOESY spectrum.

The distances were converted to constraint energies:

$$E = \text{WNOE}(kT/2)[(R - R_0)/\delta R]^{\text{ENOE}}$$

with WNOE = a weighting factor with values of 0.01–3.0, k = the Boltzmann constant, T = the absolute temperature (300 K regardless of the effective temperature of the dynamics simulation), R = the distance between two protons in the structure or the $\langle r^{-6}\rangle^{1/6}$ average distance between groups of protons in topologically equivalent groups, R_0 = the distance derived from experimental NOEs, δR = the experimental uncertainty in the distance (different values of δR can be used for $R < R_0$ and $R > R_0$), and ENOE = an exponent with values of 2 or 4. The overall root mean square (rms) fit of a structure to the NOEs was computed from the differences between R and R_0.

Structural optimizations were begun from fully extended conformations and the NOE constraints slowly phased in. The point that gave the lowest energy structure from previous dynamics trajectories of 400 ps at 1000 K which had WNOE = 0.1, ENOE = 2 (Madison et al., 1988) was used as the starting point for the current optimizations. Each run had four dynamics steps at 1000 K: (a) WNOE = 0.3, ENOE = 2; (b) WNOE = 3.0, ENOE = 2; (c) WNOE = 0.6, ENOE = 4; (d) WNOE = 3.0, ENOE = 4; each of the steps covered 5 ps except in the first run steps a and b were 15 ps each; step a of run $n + 1$ follows step d of run n. Additional steps included: (e) dynamics quenching from 1000 K to near 0 K in 15 ps with WNOE = 3.0, ENOE = 4; (f) minimization with WNOE = 3.0, ENOE = 4; and (g) minimization with WNOE = 1.0, ENOE = 4. The optimized structures from step g were used in subsequent analyses. Peptide groups were constrained to be planar-trans throughout the optimization except for step g.

For each peptide, the 40 or more conformations optimized by using distance constraints were analyzed for global and local similarities based on rms fits of α-carbons in the peptide backbone. Local structures (turns, helices, etc.) were identified by (1) aligning each segment of four or seven consecutive α-carbons with the corresponding segment in the lowest energy conformer, (2) computing the average coordinates for each segment, and (3) realigning each segment with the average segment and computing the rms fit. Global comparisons were made by using all α-carbons in the peptide backbone. First, the conformers were sorted in order of increasing energy. The lowest energy conformer was the first member of the first family. The next conformer was added to the first if it fitted within the specified rms cutoff (generally 1–5 Å); otherwise it became the first member of the second family. Each subsequent conformer was compared to the defined families in order and became a member of the first family which it fitted within the cutoff; otherwise it was placed in a new family. The resultant family classification has ordered the lowest energy representatives of each structural type. These representatives were compared graphically.

Results and Discussion

Design of VIP Analogue. Throughout the course of our synthetic work on VIP analogues, we were aware that the native molecule possessed a region of residues with high helical potential. Secondary structure algorithms (Chou & Fasman, 1978) predicted a helical segment spanning residues 12–20. On the basis of the conformational propensities described by Chou and Fasman (1978), it was calculated that replacement of the arginine residues at positions 12 and 14 by lysine residues would enhance the helical character of the 12–20 segment. Values of $\langle P_\alpha\rangle = 1.17$ and $\langle P_\beta\rangle = 1.03$ for this segment in native VIP would change to $\langle P_\alpha\rangle = 1.21$ and $\langle P_\beta\rangle = 0.94$ for the Lys^{12},Lys^{14} replacement. This prediction, along with other structure–activity information, led to the synthesis of the analogue VIP′. The helicity of VIP′ in solution was found to be no greater than that of native VIP (Table I). However, the activity of VIP′, when assayed for airway smooth muscle relaxation on guinea pig tracheal rings, was 10 times higher than that of native VIP (Bolin et al., 1988).

CD Spectroscopy. The CD spectra of native VIP and of VIP′ were obtained at various relative concentrations of methanol/water, at two pH values. Mean residue ellipticity values are shown in Table I. Calculations of secondary structure content from these spectra showed that the extents of helicity of VIP and VIP′ increase comparably with increases in methanol concentration (Table I). The pH appeared to have

Table I: CD Spectroscopy of Native VIP and the Analogue VIP'

peptide[a]	% MeOH	pH 4		pH 6	
		m_θ[b]	% helix[c]	m_θ	% helix
VIP	0	−3600	5	−6000	10
	25	−15000	40	−16000	45
	50	−20000	60	−23000	70
VIP'	0	−2000	0	−4000	5
	25	−9100	20	−13000	35
	50	−22000	65	−22000	65

[a] Peptide concentration = 2×10^{-5} M in 50 mM phosphate buffer. [b] Mean residue ellipticity at 222 nm (calculated as molar ellipticity/number of residues). [c] Calculated according to Chen et al. (1972).

little effect on the helical content of VIP' (Table I).

NMR Spectroscopy: Assignment of Resonances. NMR studies were performed on VIP' in 25% methanol and in 50% methanol. Low pH values were utilized in order to minimize exchange broadening of NH resonances. In 25% methanol, rapid NH exchange at pH 6 resulted in inferior NOESY spectra; therefore, conformational studies were performed at pH 4. In 50% methanol, the peptide was not readily soluble below pH 6. At pH 6, NH exchange was generally slower than in 25% methanol, and high-quality NOESY spectra were obtainable.

Resonances were assigned by using 2-D methods. The assignment techniques utilized were those pioneered by Wüthrich and co-workers (Wüthrich, 1986) and refined in recent studies of small proteins (Weber et al., 1985a; Holak & Prestegard, 1986; Klevit et al., 1986). The strategy was to first identify protons of the same residue by tracing connectivity patterns in COSY and relay–COSY spectra and to classify the residues by type on the basis of these patterns and by comparison to chemical shifts derived from model peptides (Bundi & Wüthrich, 1979; Wüthrich, 1986). The next step was to use NOEs among backbone protons from NOESY spectra to find which residues were likely to be neighbors and thereby identify each residue specifically by number with reference to the primary sequence.

The region of NH–C_αH cross-peaks in the COSY spectrum, the so-called "fingerprint", was used as the starting point for tracing J connectivities for each residue. All but one of the expected 28 cross-peaks were resolved for the peptide in 25% methanol, pH 4.0, and in 50% methanol, pH 6.0; all 28 were observable for the peptide in 25% methanol, pH 6.0. There were minor shifts in the positions of cross-peaks for the 25% methanol sample upon increasing the pH; however, the changes resulting from an increase in methanol concentration to 50% (Figure 1) were so widespread that these two fingerprint regions had to be assigned by tracing further connectivities for each—they could not be matched in a direct comparison.

In the COSY spectrum of VIP' in 50% methanol, unambiguous C_αH–C_βH cross-peaks were found for 19 of the residues. There were three situations in which multiple C_αH–C_βH cross-peaks could not be assigned due to overlapping C_αH chemical shifts: Thr[7]/Ala[18], Tyr[22]/Ser[25]/Leu[27], and Nle[17]/Leu[23]/Val[26] (as later assigned). These uncertainties were resolved in the relay–COSY experiments: cross-peaks were seen directly connecting C_βH protons to NH protons for all of the eight residues in question. The remaining residue, Thr[28], was assigned by default from the remaining C_βH–$C_\gamma H_3$ COSY cross-peak. Overlap of its C_αH and C_βH resonances explained the absence of C_αH–C_βH COSY, and C_αH–$C_\gamma H_3$ and NH–C_βH relay–COSY, cross-peaks for this residue.

The process of assigning each identified NH–C_αH–C_βH set in terms of residue type involved tracing further connectivities and evaluation of the C_βH chemical shift values. C_βH chemical shift criteria and the known amino acid composition were used to separate the sets into five classes: serine or threonine (4.2–3.6 ppm); aromatic (3.3–2.9 ppm); aspartate or asparagine (2.9–2.6 ppm); glutamine, valine, lysine, leucine, or norleucine (2.4–1.7 ppm); and alanine (1.6–1.3 ppm).

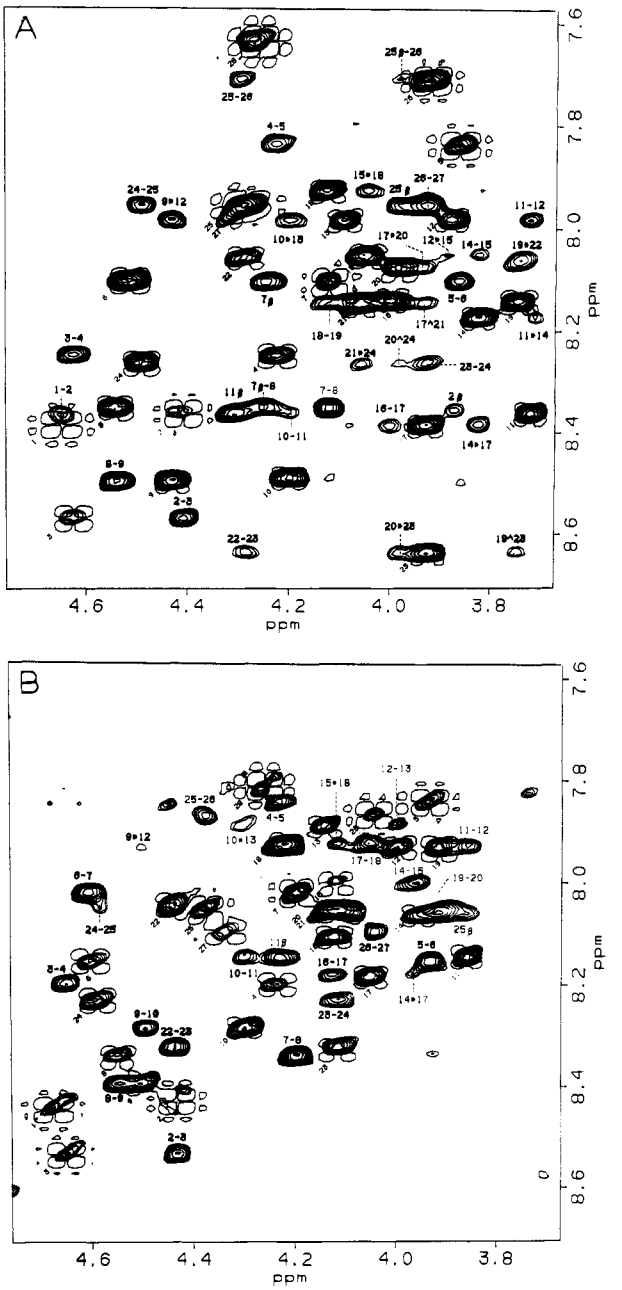

FIGURE 1: Combined plot of the "fingerprint" regions of COSY and NOESY spectra for VIP' in (A) 50% methanol, pH 6.0 and (B) 25% methanol, pH 4.0. The NOESY mixing time for each was 0.2 s. COSY $C_\alpha H_i$–NH_i cross-peaks appear as single-contour "cloverleafs", with equivalent positive and negative contours plotted. They are identified by sequence number, labeled with small numbers at −45° angles. The NOEs are generally multicontoured, with successive levels plotted geometrically, by use of a factor of 1.3. Paired numbers separated by a (−) ($i - i+1$) identify sequential $C_\alpha H_i$–NH_{i+1} NOEs; those separated by a (*) ($i * i+3$) identify $C_\alpha H_i$–NH_{i+3} NOEs; those separated by a (∧) ($i \wedge i+4$) identify $C_\alpha H_i$–NH_{i+4} NOEs. Single numbers with β (i_β) identify intraresidue $C_\beta H_i$–NH_i NOEs. Paired numbers with β ($i_\beta - i+1$) identify sequential $C_\beta H_i$–NH_{i+1} NOEs. Intraresidue $C_\alpha H_i$–NH_i NOEs are not labeled but can be identified by their positions in the center of the COSY "cloverleafs".

Resonances of threonine were readily differentiated from those of serine by the following observations: the C_βH resonances of Thr[7] and Thr[11] were at lower field than the C_αH resonances, which is expected for threonine, but not serine,

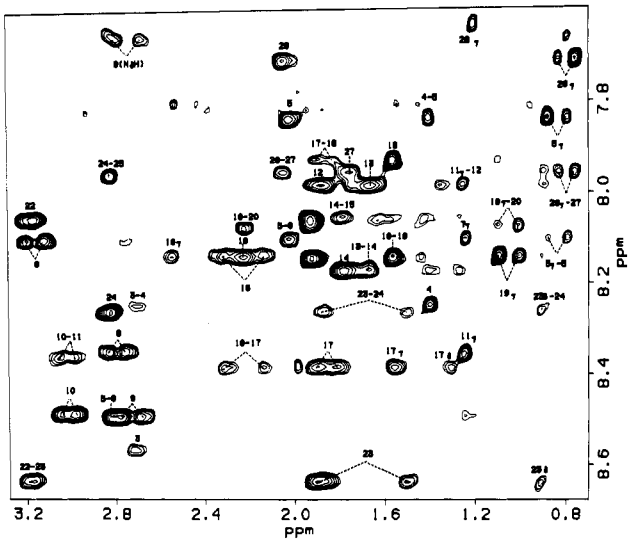

FIGURE 2: NH–$C_{aliphatic}$H region of NOESY spectrum for VIP′ in 50% methanol. The mixing time was 0.2 s. Successive levels are plotted geometrically, by use of a factor of 1.4. Single numbers (i) identify intraresidue $C_\beta H_i$–NH_i NOEs. Paired numbers ($i - i+1$) identify sequential $C_\beta H_i$–NH_i+1 NOEs. Single numbers with γ or δ ($i_{\gamma,\delta}$) identify intraresidue $C_\gamma H_i$–NH_i or $C_\delta H_i$–NH_i NOEs. Paired numbers with γ or δ ($i_{\gamma,\delta} - i+1$) identify interresidue $C_\gamma H_i$–NH_{i+1} or $C_\delta H_i$–NH_{i+1} NOEs. The symbol $N_\delta H$ indicates an intraresidue $C_\beta H_i$–$N_\delta H_i$ effect for Asn[9].

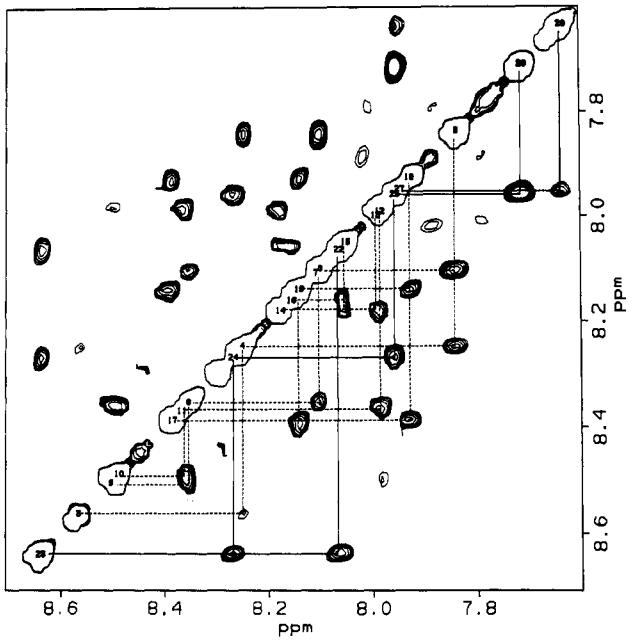

FIGURE 3: NH–NH region of NOESY spectrum for VIP′ in 50% methanol. The mixing time was 0.2 s. Successive levels are plotted geometrically, by use of a factor of 1.3. The positions of NH resonances are identified by sequence number along the diagonal. NH_i–NH_{i+1} NOEs are indicated by dotted lines for residues 3–18 and by solid lines for residues 19–28.

residues; cross-peaks were seen in COSY spectra linking the C_βH of Thr[7] and Thr[11] to $C_\gamma H_3$ resonances; overlaps in the $C_\beta H$–$C_\gamma H_3$ region were resolved, and assignments confirmed, by $C_\alpha H$–$C_\gamma H_3$ cross-peaks in the relay–COSY spectra. The threonine residues also characteristically exhibited NOEs between the NH and $C_\gamma H_3$ resonances (Figure 2). A strong cross-peak was observed between the NH and $C_\gamma H_3$ protons for Thr[28] in the relay–COSY spectra; such unexpected long-range connectivities have been described previously for other residue types (Kay et al., 1987).

Differentiation among the aromatic residues, and between aspartate and asparagine, was accomplished in the following manner: the ring protons of the aromatic residues and the side-chain NH_2 protons of the asparagine residues were assigned on the basis of chemical shift and COSY connectivities; the ring C2,C6H and side-chain NH_2 resonances were then linked to $C_\beta H$ resonances by NOEs; confirmatory NOEs were also observed from the ring C2,C6H protons to the $C_\alpha H$ proton for Tyr[10] and Tyr[22], and to the NH proton for Phe[6].

The glutamine residue was readily assigned on the basis of its unique $C_\beta H$–$C_\gamma H$ COSY cross-peaks; its side-chain NH_2 protons gave no NOEs to the $C_\gamma H$ resonances, but were assigned by default following identification of the asparagine NH_2 resonances.

Valine residues were assigned on the basis of $C_\beta H$–$C_\gamma H_3$ COSY cross-peaks. These assignments were confirmed by $C_\alpha H$–$C_\gamma H_3$ cross-peaks in the relay–COSY spectrum. All three valines were further characterized by NOEs between the NH and $C_\gamma H_3$ resonances (Figure 2).

The remaining lysine, leucine, and norleucine residues could not be fully distinquished in COSY or relay–COSY spectra due to overlap of side-chain $C_\beta H$ and $C_\gamma H$ protons. The norleucine methyl resonance was assigned on the basis of its COSY cross-peak to a $C_\gamma H_2$ resonance located at higher field than that expected for a leucine $C_\gamma H$ proton. NOEs between $C_\alpha H$ resonances and leucine $C_\delta H_3$ resonances were used to tentatively assign the three leucine residues.

An analogous set of experiments and assignment procedures was performed for the peptide in 25% methanol at pH 4.0. Problems due to overlap were resolved by using relay–COSY spectra as described, although in this sample different sets of residues exhibited overlap.

The assigned residues were next identified by specific sequence number on the basis of NOEs among backbone $C_\alpha H$ and NH protons. Model studies and surveys of protein X-ray structures have shown that, for all sterically allowed values of the dihedral angles ϕ and ψ along a peptide backbone, the NH proton of a given residue should be <3.4 Å from either the $C_\alpha H$ or NH of its N-terminal neighbor (Billeter et al., 1982). The useful consequence for NMR is that every NH should exhibit an NOE to a neighboring $C_\alpha H$ or NH proton. Numerous factors may prevent the development or observation of these NOEs, such as local flexibility or averaging of multiple conformations (Braun et al., 1981). In addition, one expects to observe a significant number of NOEs between nonneighboring residues (Wüthrich et al., 1984). However, it has been shown that the NOEs observed in a peptide or small protein are sufficient to provide a unique, self-consistent set of assignments if it is assumed that most of the effects are due to interproton proximities expected for standard secondary structures, and if the remaining "long-range" effects can all be accommodated by a single tertiary structure (Williamson et al., 1985; Wüthrich, 1986).

Thus, sequential assignments for VIP′ were made by using $C_\alpha H$–NH and NH–NH NOEs to identify neighboring residues, on the basis of the previous assignments by residue type and the amino acid sequence of the peptide. The observed sequential NOEs for VIP′ are shown in Figures 1 and 3 and summarized in Figure 4. Potential uncertainties, created by the presence of overlapping $C_\alpha H$ or NH chemical shifts, never involved more than three consecutive residues and were resolved in the process of discerning the single set of assignments that accommodated all of the NOE data. This assignment scheme was further confirmed by its ability to explain all of the nonsequential NOEs (Figure 4, Table II) as effects compatible with common secondary structures, such as the numerous $C_\alpha H_i$–NH_{i+3} and $C_\alpha H_i$–$C_\beta H_{i+3}$ NOEs, which are

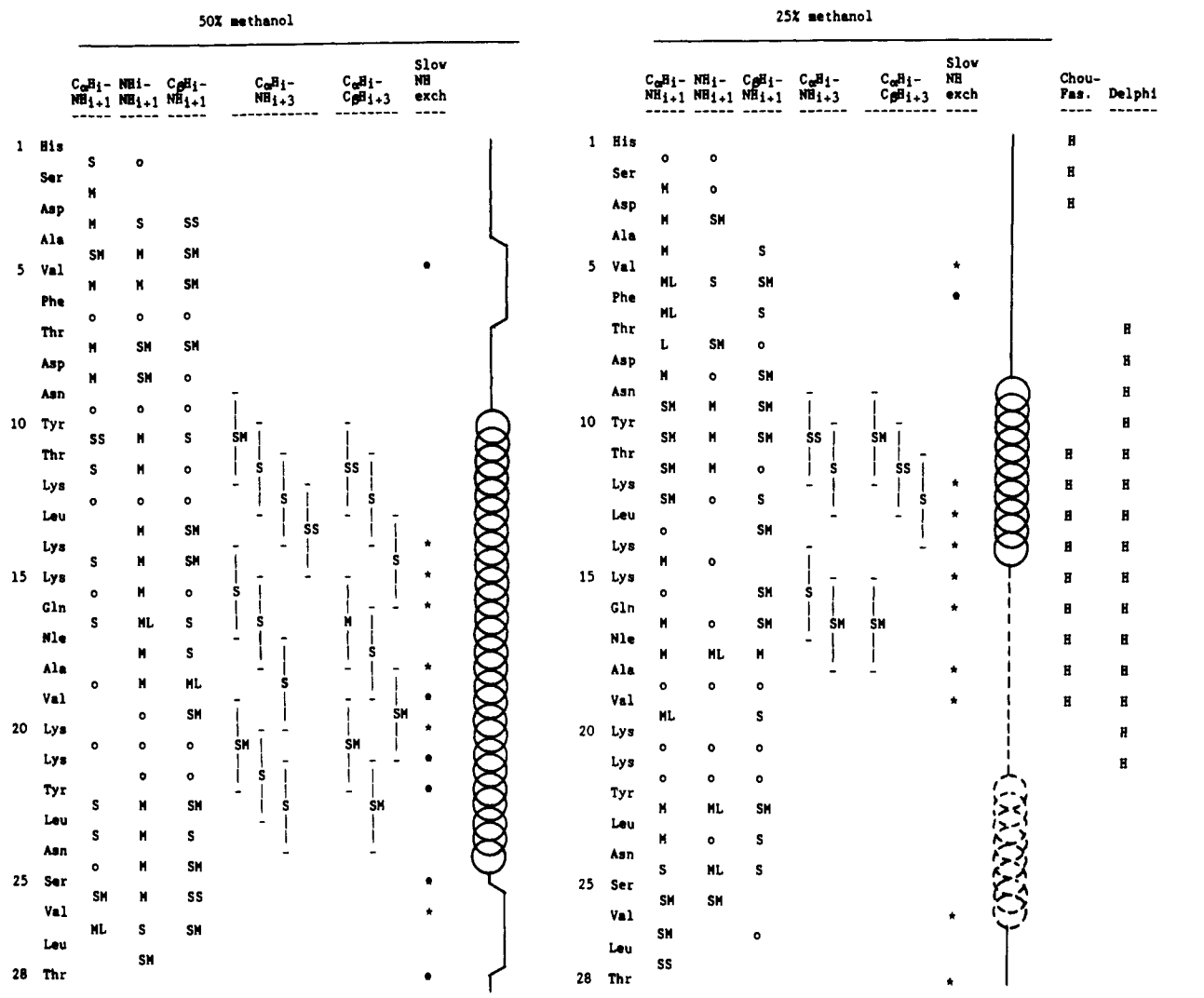

FIGURE 4: Sequential and long-range helical NOEs, NH exchange rates, structural assessments, and structural predictions for VIP′ in 50% methanol and 25% methanol. NOEs are indicated by using the size code described in the text (Experimental Procedures). The symbol (o) denotes a situation in which an NOE either could not be observed or could not be quantitated, due to overlap with the diagonal or with another NOE. An asterisk (*) indicates a slow NH exchange rate. The exchange rate was deemed slow if the water saturation-transfer experiment (see Experimental Procedures) produced little or no measurable reduction in the size of the NH resonance. An assessment of the structure of VIP′, based on the NMR results alone, is given symbolically for each solvent where a straight line = extended; a hump in the straight line = turn; linked circles = α-helix; broken linked circles = possible irregular helix; and a broken straight line = could not be determined from the NMR results. The symbols (H) in the columns representing predicted structure indicate regions of VIP′ where a high probability exists for α-helix formation: i.e., a positive $\{\langle P_\alpha \rangle - \langle P_\beta \rangle\}$ value in the three-state model of Chou and Fasman (1978) or a large α probability factor (above "safe" cutoff) in the Delphi algorithm (Garnier et al., 1978).

typically found in an α-helix.

Although full sequential assignments were made for each sample, there were numerous NOEs that could not be uniquely assigned or accurately quantitated due to overlap (Figure 4). For example, the NH resonances of Phe[6] and Thr[7] had identical chemical shifts, and a $C_\alpha H_i$–NH_{i+1} NOE between them would have been indistinguishable from an intraresidue $C_\alpha H_i$–NH_i effect for Phe[6] (Figure 1A). Interestingly, in 25% methanol these NH resonances did not overlap, and both the interresidue and intraresidue effects were observed (Figure 1B). A comparable set of circumstances was found for Asn[9] and Tyr[10] (Figure 1).

The chemical shift assignments for VIP′ in 50% methanol, and the chemical shifts of resonances that were significantly different in 25% methanol, are given in Table III.

NMR Spectroscopy: Assessment of Secondary Structure. It has been shown (Williamson et al., 1984; Weber et al., 1985a; Holak & Prestegard, 1986; Klevit & Waygood, 1986; Wüthrich, 1986) that patterns of NOE connectivities in peptides and small proteins can be diagnostic of regions of secondary structure. Extended or β-strand regions typically produce large $C_\alpha H_i$–NH_{i+1} NOEs; α-helices typically produce NH_i–NH_{i+1} and $C_\beta H_i$–NH_{i+1} effects, and possibly $C_\alpha H_i$–NH_{i+3} and $C_\alpha H_i$–$C_\beta H_{i+3}$ effects; turns produce various characteristic combinations of NOEs (Wüthrich et al., 1984; Wüthrich, 1986). The NOE patterns observed in VIP′ were interpreted in terms of proposed secondary structure, as shown in Figure 4. In 50% methanol, VIP′ adopts a clearly identifiable α-helix at residues 10–25, with possible turns at residues 4–7 and 25–28. In 25% methanol, residues 2–8 are most likely extended; 9–14 appear to be helical; 22–26 may be in an irregular helix; and the structure at residues 15–21 cannot be ascertained.

Reduced rates of exchange of NH protons with solvent H_2O may be indicative of hydrogen bonding and/or shielding due to tertiary structure (Hvidt & Nielsen, 1966; Englander et al., 1972; Krishna et al., 1979; Qiwen et al., 1987). In VIP′, slowly exchanging NH protons were identified from water saturation-transfer experiments (Figure 4). Although most of the slowly exchanging protons appeared to be located in structured

Table II: Nonstandard Interresidue NOEs for VIP′

	size[a]
50% Methanol	
$C_\gamma H_f$–NH_{i+1}	
Val[5] $C_\gamma H_3$–Phe[6] NH	S
Thr[11] $C_\gamma H_3$–Lys[12] NH	SM
Val[19] $C_\gamma H_3$–Lys[20] NH	S
Val[26] $C_\gamma H_3$–Leu[27] NH	S
$C_\alpha H_f$–NH_{i+4}	
Nle[17] $C_\alpha H$–Lys[21] NH	S
Val[19] $C_\alpha H$–Leu[23] NH	SS
Lys[20] $C_\alpha H$–Asn[24] NH	SS
other	
Leu[23] $C_\delta H_3$–Asn[24] NH	S
Gln[16] $C_\alpha H$–Val[19] $C_\gamma H_3$	SM
Val[5] $C_\gamma H_3$–Asn[9] NH_2	S
Val[5] $C_\gamma H_3$–Phe[6] ring C2,C6H	S
Thr[7] $C_\alpha H$–Phe[6] ring C2,C6H	S
Thr[7] $C_\gamma H_3$–Phe[6] ring C2,C6H	S
Thr[11] $C_\gamma H_3$–Tyr[10] ring C2,C6H	SS
Thr[11] $C_\gamma H_3$–Tyr[10] ring C3,C5H	SS
Val[19] $C_\alpha H$–Tyr[22] ring C2,C6H	SS
Lys[21] $C_\beta H_2$–Tyr[22] ring C2,C6H	S
Leu[23] $C_\alpha H$–Tyr[22] ring C2,C6H	S
Leu[23] NH–Tyr[22] ring C2,C6H	SS
Leu[23] $C_\delta H_3$–Tyr[22] ring C2,C6H	SM
Leu[23] $C_\delta H_3$–Tyr[22] ring C3,C5H	SM
Val[26] $C_\gamma H_3$–Tyr[22] ring C2,C6H	S
Val[26] $C_\gamma H_3$–Tyr[22] ring C3,C5H	SM
25% Methanol	
$C_\gamma H_f$–NH_{i+1}	
Val[19] $C_\gamma H_3$–Lys[20] NH	SM
other	
Val[26] $C_\gamma H_3$–Tyr[22] ring C2,C6H	SM
Val[26] $C_\gamma H_3$–Tyr[22] ring C3,C5H	SM

[a] Distances corresponding to the size code are given in the text (Experimental Procedures). Where resolved NOEs were observed to resonances that were resolved but not stereospecifically assigned, the largest value has been listed.

regions, they were not fully distributed throughout each proposed element of secondary structure (Figure 4). The distribution may indicate localized rigidity or surface inaccessibility of the backbone in each structural region.

Coupling constants, which may be useful in assessing secondary structure, could not be accurately measured in 1-D spectra due to overlap, nor in 2-D spectra due to low resolution.

Dynamics and Minimization: Refinement of Protocol. A constrained dynamics and minimization protocol (Experimental Procedures) was developed that readily folded peptides to give conformers in accord with the CD and NMR data, while affording an assessment of the degree of uncertainty in the structural determination at each peptide segment. This protocol was selected by exploring the effects of various computational parameters as summarized below for VIP′ in 50% methanol [see Madison et al. (1988) for details]. When the full formal charges (±1) were used for the two Asp and five Lys side chains and the secondary structure model from the NMR data was used as a starting conformation, the α-helical structure indicated by the CD and NMR experiments (>50% helix content) collapsed, due to the dominance of interactions with the charged side chains. However, the secondary structure was retained when reduced formal charges and a dielectric constant of r were used as an approximation for the attenuation of interactions of the charged groups due to solvation. Qualitatively similar VIP′ structures were obtained with formal charges of ±0.0, 0.25, or 0.50. Formal charges of ±0.25 were used subsequently.

A type III β-turn was obtained for residues 3–6 in optimizations with WNOE = 1.0 and 25.0, but not in two separate optimizations with WNOE = 0.1. In an optimization with

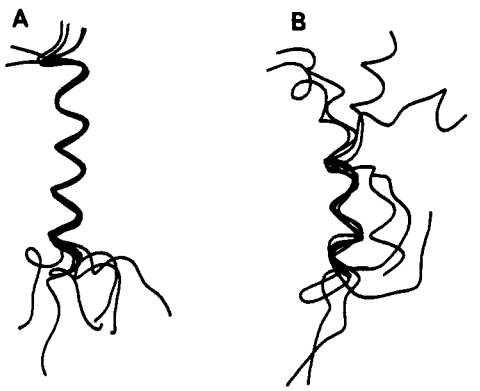

FIGURE 5: Single-stranded ribbon spline fit to the peptide backbone of the lowest energy member for each of the first five or six structural families for VIP′. The N-termini are toward the bottom and the C-termini toward the top. The solvent and the segment which were overlapped for the plot: (A) 50% methanol, residues 10–25; and (B) 25% methanol, residues 10–18.

WNOE = 1.0, a unique, nonclassical kink for residues 10–13 was retained throughout the simulation, but this segment was α-helical in three other optimizations. Using WNOE = 0.1 permitted conformational flexibility during the simulation but failed to produce good agreement with the experimental distances (rms deviations up to 1.0 Å were observed). When starting from a fully extended structure, the covalent structure was significantly distorted throughout the simulation unless the NOE constraints were phased in slowly.

For the final protocol (Experimental Procedures) a key factor in obtaining good fits to the NOE data was increasing the exponent (ENOE) from 2 to 4 in the equation for the constraint energy. The exponent of 4 heavily penalizes large deviations from the target distance, but still permits variations within the error range. The lower values of WNOE and ENOE at the beginning of each run permit flexibility rather than locking the peptide into a particular structure. For the dynamics and the minimization, slowly phasing in the NOE constraints is essential to avoid obtaining a distorted, high-energy structure.

Dynamics and Minimization: Assessment of Secondary and Tertiary Structure. The optimization protocol readily folds VIP′ from the fully extended conformation to conformers that satisfy all of the distance constraints derived from the experimental NOEs. The rms fit between the calculated and observed distances ranges from 0.31 to 0.46 Å (Table IV), well within the estimated error of 0.5 Å. Of the 139 pairwise distances for VIP′ in 25% methanol, none deviate from the observed values by more than twice the estimated error. In 50% methanol, two or three distances out of 189 deviate by slightly more than twice the estimated error for each family.

Classification of the peptide structures into low-energy families on the basis of the rms fit of all α-carbons to 2.5 Å shows that a single family contains nearly half of the conformers in 50% methanol. The greater variation in the structures in 25% methanol is indicated by the larger cutoff of 5.0 Å and the spreading of the population among the first four families (Table IV).

In 50% methanol, the C-terminal two-thirds of the peptide is α-helical for each of the families, but the position of the N-terminal third of the peptide varies considerably with respect to the helix (Figure 5). The central third of the peptide is helical in 25% methanol, but both ends vary. The N-terminal third is largely extended, while the C-terminal third contains an α-helical segment. The significant differences outside of the main helical segment illustrate the variety of structures that are consistent with the data.

Table III: Proton NMR Assignments for VIP′ in 50% CD_3OH/50% H_2O, pH 6.07 at 22.5 °C, and $\Delta\delta$ in 25% CD_3OH/75% H_2O, pH 3.95[a]

		NH	$C_\alpha H$	$C_\beta H$	$C_\gamma H$	$C_\delta H$	$C_\epsilon H$	other	
1	His	8.38 (+0.07)[b]	4.65	3.19				ring C2H:	8.31 (+0.59)
				3.07				ring C4H:	7.16 (+0.13)
2	Ser	8.36 (+0.08)	4.41	3.88					
				3.81					
3	Asp	8.56	4.62	2.72					
4	Ala	8.25	4.22	1.40					
5	Val	7.84	3.86	2.02	0.84				
					0.79				
6	Phe	8.10	4.51 (+0.10)	3.19				ring C2,C6H:	7.26
				3.12				ring C3,C5H:	7.25
								ring C4H:	7.17
7	Thr	8.10 (−0.08)	4.12 (+0.08)	4.25	1.25				
8	Asp	8.35	4.54	2.82					
				2.75					
9	Asn	8.50 (−0.10)	4.43 (+0.07)	2.79				NH2:	7.67
				2.68					6.97
10	Tyr	8.48 (−0.19)	4.20 (+0.10)	3.04				ring C2,C6H:	7.08
				2.98				ring C3,C5H:	6.78
11	Thr	8.36 (−0.21)	3.72 (+0.12)	4.31 (−0.08)	1.26				
12	Lys	7.98	3.88 (+0.10)	1.90	*c*	*d*	*e*		
13	Leu	7.98 (−0.08)	4.09	1.75	1.65	0.89			
				1.66					
14	Lys	8.17 (−0.09)	3.82 (+0.13)	1.78	*c*	*d*	*e*		
15	Lys	8.05	4.04 (+0.08)	1.93	*f*	*d*	*e*		
16	Gln	8.14	4.00 (+0.12)	2.32	2.55 (−0.13)			NH2:	7.42
				2.14					6.80
17	Nle	8.38 (−0.19)	3.93 (+0.11)	1.90	1.56 (−0.16)	1.31	0.86		
				1.82					
18	Ala	7.93	4.12 (+0.09)	1.57 (−0.09)					
19	Val	8.14 (−0.20)	3.74 (+0.16)	2.22 (−0.07)	1.09				
					1.01				
20	Lys	8.08	3.98 (+0.13)	1.92 (−0.15)	*f*	*d*	*e*		
21	Lys	8.15 (−0.09)	4.06	1.91 (−0.14)	*f*	*d*	*e*		
22	Tyr	8.06	4.28 (+0.16)	3.20				ring C2,C6H:	7.04
				3.16				ring C3,C5H:	6.73
23	Leu	8.64 (−0.30)	3.92 (+0.19)	1.88	1.91 (−0.18)	0.91			
				1.50					
24	Asn	8.26	4.49 (+0.11)	2.82				NH2:	7.65
									6.88
25	Ser	7.95 (+0.11)	4.29 (+0.09)	3.98					
				3.93					
26	Val	7.71 (+0.16)	3.92 (+0.12)	2.05	0.82				
					0.76				
27	Leu	7.95 (+0.15)	4.27 (+0.07)	1.95	1.73	0.90			
				1.57		0.87			
28	Thr	7.63 (+0.19)	4.26	4.27	1.21				
								N-Ac CH3:	2.00
								term NH2:	7.24
									7.15
								methanol:	3.31

[a] Chemical shifts are reported with respect to external DSS. [b] Values in parentheses are differences in chemical shifts, in ppm, observed in 25% CD_3OH/75% H_2O, pH 3.95 22.5 °C, reported such that $\delta_{50\%}$ + (value) = $\delta_{25\%}$. [c] Within the range 1.25–1.60. [d] Within the range 1.60–1.70. [e] Within the range 2.80–3.00. [f] Within the range 1.40–1.65.

Table IV: Low-Energy Families for VIP′ in Solution

solvent	runs[a]	NOEs[b]	cut[c] (Å)	fam[d]	mem[e]	*E*[f] (kcal/mol)	rms[g] (Å)	not fit[h]
50% methanol	44	189	2.5	1	20	−54.3	0.46	2
				2	2	−48.4	0.45	3
				3	2	−45.6	0.46	3
				4	1	−44.1	0.45	2
				5	5	−40.9	0.46	3
				6	6	−40.3	0.45	2
25% methanol	40	139	5.0	1	9	−106.8	0.33	0
				2	5	−102.7	0.33	0
				3	6	−99.5	0.33	0
				4	8	−98.9	0.35	0
				5	3	−95.3	0.31	0

[a] Runs: number of runs, i.e., number of minimized structures. [b] NOEs: number of pairwise distance constraints from NOEs. [c] Cut: cutoff for family classification. [d] Fam: family number. [e] Mem: number of members in that family. [f] *E*: energy of peptide structure (without constraint energy). [g] rms: rms deviation between interproton distances and target distance from NOEs. [h] Not fit: number of interproton distances not fit to within twice the estimated error range.

The 40 plus optimized VIP′ structures for each solvent were further analyzed for local structural elements involving at least four residues. Regions with average rms <0.5 Å correspond to defined structural segments, while regions with larger values

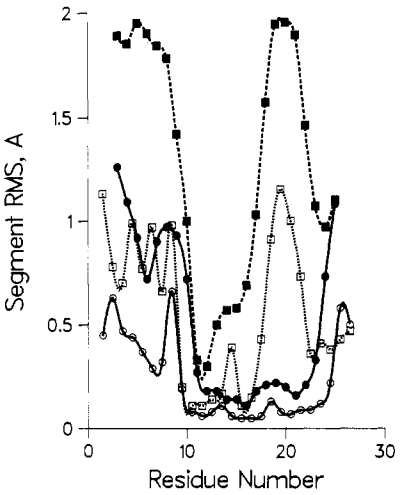

FIGURE 6: Average rms for fit of consecutive segments of α-carbons to the average segment for the 40 plus optimized VIP′ structures. The values are plotted with the central residue on the abscissa. The solvent and number of carbons: 25% methanol, 4 C_α (□); 25% methanol, 7 C_α (■); 50% methanol, 4 C_α (○); 50% methanol, 7 C_α (●).

indicate multiple conformers within the ensemble. Root mean square fitting of successive segments of four α-carbons reveals that VIP′ is well-ordered from residues 8–26 in 50% methanol and has a short segment of moderate order centered at residue 6, but has multiple conformers at both ends of these segments (Figure 6). Similarly, VIP′ in 25% methanol is well-ordered from residues 8–18 and moderately ordered from residues 21–28. The N-terminal third and a hinge region centered at residue 20 have multiple conformers. The extent of the ordered segments is reflected by the rms values for seven successive α-carbons. The long segment comprised of residues 8–26 for VIP′ in 50% methanol is well-ordered over its entire length. By contrast, only the 8–15 segment has comparable order for VIP′ in 25% methanol. The effectiveness of the present protocol in exploring multiple conformations is illustrated by the fact that the segment rms in the unordered regions is as high as for simulations in which WNOE was 0.1 and ENOE was 2 throughout (not shown).

Examination of the low-energy structures reveals that the ordered segments are largely α-helical (Figures 5 and 6). In 50% methanol, there is a type III β-turn comprising residues 5–8. In 25% methanol, the N-terminal third is largely extended but the high rms values reflect the great variety of conformations for this segment.

The optimized structures are in good accord with the CD and NMR data (Table I, Figure 4). In 50% methanol 19 residues (65%) are helical and the helical region (residues 8–26) corresponds to the original estimate from NMR data (residues 10–25). This helical segment also corresponds to Chou–Fasman and Delphi calculations (Chou & Fasman, 1978; Garnier et al., 1978) (Figure 4) which predicted the highest potential for α-helix formation at residues 13–18. Two possible β-turns at residues 4–7 and 25–28 were suggested by the NMR data. In the optimization a type III turn is observed at residues 5–8 while the latter turn tends to merge with the helical segment. In 25% methanol the optimization gave two irregular helical segments of nine (residues 9–17) and six (residues 23–28) residues which are separated by a hinge region. Fifteen helical residues corresponds to 50%, but the helical content measured by CD would be reduced by the shortness and irregularity of the helical segments. The initial analysis of the NMR data assigned residues 9–14 as helical and 22–26 as a potential, irregular helix, but the 15–21 segment was indeterminate from the pattern of NOEs.

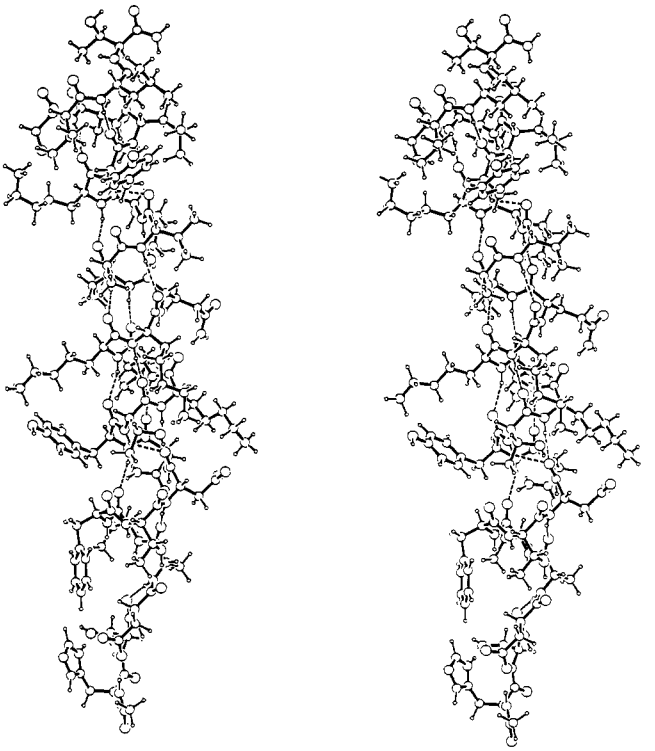

FIGURE 7: Stereo ORTEP plot for the lowest energy optimized conformer for VIP′ in 50% methanol. The N-terminus is toward the bottom.

The side-chain and backbone conformations of the lowest energy structure for VIP′ in 50% methanol (Figure 7) are representative for family 1. A number of features involving residues that seem to be critical to bioactivity are conserved throughout the structural families in both 25% and 50% methanol. These features include a cluster of the side chains of Asp^3, Phe^6, Thr^7, and Tyr^{10} near the N-terminus and a second cluster of residues Ala^{18}, Val^{19}, Tyr^{22}, Ile^{23}, Val^{26}, and Ile^{27} near the C-terminus. A hydrogen bond from the Thr^7 side chain to the backbone carbonyl oxygen of Asp^3 (present in the optimized structures only in 50% methanol) may help hold these residues in proximity. A helical segment may be stabilized by a hydrogen bond between the side chains of Asp^8 and Lys^{12} in both solvents (Marqusee & Baldwin, 1988).

Solvent-Dependent Changes in Peptide Conformation. VIP′ in 25% methanol exhibited no major conformational change upon a change in pH from 4 to 6, as assessed by CD. In NMR spectra, this pH change was accompanied by chemical shift differences for residues in two regions—those near His^1, which was being titrated over this pH range as monitored by chemical shift changes of its ring protons (not shown); and residues 8–12, which may indicate sensitivity to the protonation state of either the His^1 ring or the Asp^8 side chain, although the Asp^8 $C_\beta H_2$ chemical shifts did not change significantly between the two pH values.

A change in the methanol concentration of the solvent from 25% to 50% caused extensive structural alterations in VIP′. The hinge region, residues 18–22, became helical, uniting two short, irregular helical segments into one long, regular segment.

The present study provided a closed system in which to evaluate the sensitivity of NMR parameters, other than sequential NOEs, to a structural change. We investigated whether the amino acid residues whose protons exhibited the largest changes in certain NMR parameters were located in regions of newly formed or rigidified secondary structure in VIP′ upon the change from 25% to 50% methanol. We found no obvious correlation for the intraresidue NOEs: $C_\alpha H_i$–NH_i,

$C_\beta H_i$–NH_i, and $C_\alpha H_i$–$C_\beta H_i$. Formation and rigidification of helix was primarily noted by the appearance of numerous NOEs of the $C_\alpha H_i$–NH_{i+3} and $C_\alpha H_i$–$C_\beta H_{i+3}$ type. Residues in this region also exhibited slightly larger changes in chemical shift for NH, $C_\alpha H$, and $C_\beta H$ protons (Figure 1, Table III) and reduced NH exchange rates (Figure 4). Thr^{11}, Val^{19}, and Leu^{23} exhibited exceptionally large total changes in chemical shift values. The specific structural basis of this observation is not clear.

Structure–Activity Considerations for VIP. Although determination of a receptor-bound conformation has not yet been achieved for any peptide hormone, studies of protein–protein binding interactions, such as antibody–antigen complexes (Amit et al., 1986; Colman et al., 1987), suggest that in such an association the ligand protein does not change its overall conformation significantly. Elimination of water at the protein–protein interface should create a somewhat hydrophobic environment. Therefore, the conformation preferred by a free peptide hormone in an equally hydrophobic solvent should closely approximate the biologically active conformation. We have tried to mimic the proper hydrophobic environment by using methanol/water mixtures. Of course, it is not known exactly what ratio of methanol/water corresponds to the receptor binding site. Therefore, we can conclude only that the active conformation of VIP is predominantly α-helical and that a rigid helical region is comprised of at least residues 10–15.

Sequence homology among the members of the VIP class of peptide hormones, including growth hormone releasing factor (GRF) (Guillemin et al., 1982), secretin (Bodanszky et al., 1966), glucagon (Bromer et al., 1957), peptide histidine–isoleucinamide (PHI) (Tatemoto & Mutt, 1981), helodermin (Vandermeers et al., 1987), and helospectrin (Parker et al., 1984), suggests that Phe^6 and Thr^7 are important for binding activity and that Asp^3, Tyr^{10}, and Leu^{23} are also probably involved in binding. In the low-energy structure of VIP′ in 50% methanol (family 1; Figure 7), the side chains of residues 3, 6, 7, and 10 are clustered together. Leu^{23} is in a cluster of hydrophobic side chains positioned far from the other homologous residues. This suggests that the binding area on the receptor may have two separated regions that interact with VIP.

The solution structures of glucagon in dodecylphosphocholine micelles (Braun et al., 1983), GRF in 30% trifluoroethanol (Brünger et al., 1987), and secretin in 40% trifluoroethanol (Gronenborn et al., 1987) have been determined by NMR. They are all extended throughout the N-terminal six to nine residues, and predominantly α-helical along the rest of the molecule, with a kink at residues 13–16. VIP′ exhibits a similar conformation in 50% methanol, although it has a comparable kink only in 25% methanol.

The structural information we have obtained will be used to guide the design of new analogues and mimetic versions of VIP. Structure–activity principles determined for VIP should be applicable in studies on GRF and the other homologous peptide hormones. Peptide T, a purported anti-AIDS compound (Pert et al., 1986), is also homologous to a section (residues 4–11) of VIP. In addition, we will use the behavior of VIP in various solvents to examine how α-helices are formed, and how this formation might be expedited and ultimately stabilized by amino acid replacements and chemical modification of side chains.

Acknowledgments

We thank Ross Pitcher, and Dr. Arthur Pardi of the University of Colorado, for help in optimizing the performance of the XL-400 NMR spectrometer. We are also grateful to J. Blount, A. Krohn, A. Meade, K. Mueller, H. Ammann, D. Doran, P. Gerber, G. Schrepfer, T. J. O'Donnell, and A. Olson for software.

Registry No. VIP, 40077-57-4; VIP′, 117811-28-6; methanol, 67-56-1.

References

Alm, P., Alumets, J., Hakanson, R., & Sundler, F. (1977) *Neuroscience 2*, 751–754.

Amit, A. G., Mariuzza, R. A., Phillips, S. E. V., & Poljak, R. J. (1986) *Science 233*, 747–753.

Anil Kumar, Ernst, R. R., & Wüthrich, K. (1980) *Biochem. Biophys. Res. Commun. 95*, 1–6.

Aue, W. P., Bartholdi, E., & Ernst, R. R. (1976) *J. Chem. Phys. 64*, 2229–2246.

Bax, A., & Freeman, R. (1981) *J. Magn. Reson. 44*, 542–561.

Billeter, M., Braun, W., & Wüthrich, K. (1982) *J. Mol. Biol. 155*, 321–346.

Bodanszky, M., Ondetti, M. A., Levine, S. D., Narayanan, V. L., Saltza, M. V., Sheehan, J. T., Williams, N. J., & Sabo, E. F. (1966) *Chem. Ind.* 1757–1758.

Bodanszky, M., Bodanszky, A., Klausner, Y. S., & Said, S. I. (1974) *Bioorg. Chem. 3*, 133–140.

Bolin, D. R., Sytwu, I. I., Cottrell, J. M., Garippa, R. J., Brooks, C. C., & O'Donnell, M. (1988) in *Proceedings of the Tenth American Peptide Symposium* (G. Marshall, Ed.) pp 441–443, Escom, Leiden.

Braun, W., Bosch, C., Brown, L. R., Go, N., & Wüthrich, K. (1981) *Biochim. Biophys. Acta 667*, 377–396.

Braun, W., Wider, G., Lee, K. H., & Wüthrich, K. (1983) *J. Mol. Biol. 169*, 921–948.

Bromer, W. W., Sinn, L. G., & Behrens, O. K. (1957) *J. Am. Chem. Soc. 79*, 2807–2810.

Brooks, B. R., Bruccoleri, R. E., Olafson, B. D., States, D. J., Swaminathan, S., & Karplus, M. (1983) *J. Comput. Chem. 4*, 187–217.

Brünger, A. T., Clore, G. M., Gronenborn, A. M., & Karplus, M. (1987) *Protein Eng. 1*, 399–406.

Bundi, A., & Wüthrich, K. (1979) *Biopolymers 18*, 285–297.

Chen, Y. H., Yang, J. T., & Martinez, H. M. (1972) *Biochemistry 11*, 4120–4131.

Chou, P. Y., & Fasman, G. D. (1978) *Annu. Rev. Biochem. 47*, 251–276.

Colman, P. M., Laver, W. G., Varghese, J. N., Baker, A. T., Tulloch, P. A., Air, G. M., & Webster, R. G. (1987) *Nature 326*, 358–363.

Dey, D. A., Shannon, W. A., & Said, S. I. (1981) *Cell Tissue Res. 220*, 231–238.

Eich, G., Bodenhausen, G., & Ernst, R. R. (1982) *J. Am. Chem. Soc. 104*, 3731–3732.

Englander, S. W., Downer, N. W., & Teitelbaum, H. (1972) *Annu. Rev. Biochem. 41*, 903–924.

Fournier, A., Saunders, J. K., & St. Pierre, S. (1982) *Peptides 3*, 345–352.

Fournier, A., Saunders, J. K., & St. Pierre, S. (1984) *Peptides 5*, 169–177.

Garnier, J., Osguthorpe, D. J., & Robson, B. (1978) *J. Mol. Biol. 120*, 97–120.

Gronenborn, A. M., Boverman, G., & Clore, G. M. (1987) *FEBS Lett. 215*, 88–94.

Guillemin, R., Brazeau, P. Bohlen, P., Esch, F., Ling, N., & Wehrenberg, W. B. (1982) *Science 218*, 585–587.

Hagenmaier, H., & Frank H. (1972) *Hoppe-Seyler's Z. Physiol. Chem. 353*, 1973–1976.

Holak, T. A., & Prestegard, J. H. (1986) *Biochemistry 25*, 5766–5774.

Hvidt, A., & Nielsen, S. O. (1966) *Adv. Protein Chem. 21*, 287–386.
Kaiser, E. T., Colescott, R. L., Bossinger, C. D., & Cook, P. I. (1970) *Anal. Biochem. 34*, 595–598.
Kay, L. E., Jones, P. J., & Prestegard, J. H. (1987) *J. Magn. Reson. 72*, 392–396.
Kime, M. J., & Moore, P. B. (1983) *FEBS Lett. 153*, 199–203.
Klevit, R., & Waygood, E. B. (1986) *Biochemistry 25*, 7774–7781.
Klevit, R., Drobny, G. P., & Waygood, E. B. (1986) *Biochemistry 25*, 7760–7769.
Krishna, N. R., Huang, D. H., Glickson, J. D., Rowan, R., & Walter, R. (1979) *Biophys. J. 26*, 345–366.
Madison, V. S., Berkovitch-Yellin, Z., Fry, D. C., Greeley, D. G., & Toome, V. (1988) in *Synthetic Peptides: Approaches to Biological Problems. UCLA Symposia on Molecular and Cellular Biology, New Series* (Tam, J., & Kaiser, E. T., Eds.) Vol. *86*, Alan R. Liss, Inc., New York (in press).
Marqusee, S., & Baldwin, R. L. (1988) *Proc. Natl. Acad. Sci. U.S.A. 84*, 8898–8902.
Matsuzaki, Y., Hamasaki, Y., & Said, S. I. (1980) *Science 210*, 1252–1253.
Merrifield, R. B. (1963) *J. Am. Chem. Soc. 85*, 2149–2154.
Mojsov, S., Mitchell, A. R., & Merrifield, R. B. (1980) *J. Org. Chem. 45*, 555–560.
Mueller, K., Amman, H. J., Doran, D. M., Gerber, P., & Schrepfer, G. (1986) in *Innovative Approaches In Drug Research* (Harms, A. F., Ed.) Elseier, Amsterdam.
Mutt, V., & Said, S. I. (1974) *Eur. J. Biochem. 42*, 581–589.
Parker, D. S., Raufman, J. P., O'Donohue, T. L., Bledsoe, M., Yoshida, H., & Pisano, J. J. (1984) *J. Biol. Chem. 259*, 11751–11755.
Pert, C. B., Hill, J. M., Ruff, M. R., Berman, R. M., Robey, W. G., Arthur, L. O., Ruscetti, F. W., & Farra, W. L. (1986) *Proc. Natl. Acad. Sci. U.S.A. 83*, 9254–9258.
Petterson, I., & Liljefors, T. (1987) *J. Comput. Chem. 8*, 1139–1145.
Qiwen, W., Kline, A. D., & Wüthrich, K. (1987) *Biochemistry 26*, 6488–6493.
Redfield, C., & Dobson, C. M. (1988) *Biochemistry 27*, 122–136.
Robinson, R. M., Blakeney, E. W., & Mattice, W. L. (1982) *Biopolymers 21*, 1217–1228.
Rosevear, P. R., Fry, D. C., & Mildvan, A. S. (1985) *J. Magn. Reson. 61*, 102–115.
Said, S. I. (1980) in *Gastrointestinal Hormones* (Jerzy, G., Ed.) pp 245–273, Raven, New York.
Said, S. I., & Mutt, V. (1972) *Eur. J. Biochem. 28*, 199–204.
Said, S. I., Kitmaura, S., Yoshida, T., Presnott, J., & Holden, L. D. (1974) *Ann. N.Y. Acad. Sci. 221*, 103–114.
States, D. J., Haberkorn, R. A., & Ruben, D. J. (1982) *J. Magn. Reson. 48*, 286–292.
Suzuki, Y., McMaster, D., Huang, M., Lederis, K., & Rorstad, O. P. (1985) *J. Neurochem. 45*, 890–899.
Tam, J. P., Heath, W. F., & Merrifield, R. B. (1983) *J. Am. Chem. Soc. 105*, 6442–6455.
Tatemoto, K., & Mutt, V. (1981) *Proc. Natl. Acad. Sci. U.S.A. 78*, 6603–6607.
Vandermeers, A., Gourlet, P., Vandermeers-Piret, M. C., Cauvin, A., DeNeef, P., Rathe, J., Svoboda, M., Robberecht, P., & Christophe, J. (1987) *Eur. J. Biochem. 164*, 321–327.
Waelder, S., & Redfield, A. G. (1977) *Biopolymers 16*, 623–629.
Weber, P. L., Wemmer, D. E., & Reid, B. R. (1985a) *Biochemistry 24*, 4553–4562.
Weber, P. L., Drobny, G., & Reid, B. R. (1985b) *Biochemsitry 24*, 4549–4552.
Wider, G., Macura, S., Anil Kumar, Ernst, R. R., & Wüthrich, K. (1984) *J. Magn. Reson. 56*, 207–234.
Williamson, M. P., Marion, D., & Wüthrich, K. (1984) *J. Mol. Biol. 173*, 341–359.
Williamson, M. P., Havel, T. F., & Wüthrich, K. (1985) *J. Mol. Biol. 182*, 295–315.
Wüthrich, K. (1986) *NMR of Proteins and Nucleic Acids*, John Wiley and Sons, New York.
Wüthrich, K., Billeter, M., & Braun, W. (1984) *J. Mol. Biol. 180*, 715–740.
Yoshida, T., Geumei, A. M., Schmitt, R. J., & Said, S. I. (1974) *Fed. Proc. 33*, 378.